33. Passage of Particles Through Matter

Revised August 2015 by H. Bichsel (University of Washington), D.E. Groom (LBNL), and S.R. Klein (LBNL).

This review covers the interactions of photons and electrically charged particles in matter, concentrating on energies of interest for high-energy physics and astrophysics and processes of interest for particle detectors.

Table 33.1: Summary of variables used in this section. The kinematic variables β and γ have their usual relativistic meanings.

Symbol	Definition	Value or (usual) units
$m_e c^2$	electron mass $\times\, c^2$	0.510 998 9461(31) MeV
r_e	classical electron radius $e^2/4\pi\epsilon_0 m_e c^2$	2.817 940 3227(19) fm
α	fine structure constant $e^2/4\pi\epsilon_0\hbar c$	1/137.035 999 139(31)
N_A	Avogadro's number	$6.022\,140\,857(74) \times 10^{23}$ mol^{-1}
ρ	density	g cm^{-3}
x	mass per unit area	g cm^{-2}
M	incident particle mass	MeV/c^2
E	incident part. energy γMc^2	MeV
T	kinetic energy, $(\gamma-1)Mc^2$	MeV
W	energy transfer to an electron in a single collision	MeV
k	bremsstrahlung photon energy	MeV
z	charge number of incident particle	
Z	atomic number of absorber	
A	atomic mass of absorber	g mol^{-1}
K	$4\pi N_A r_e^2 m_e c^2$ (Coefficient for dE/dx)	0.307 075 MeV mol^{-1} cm^2
I	mean excitation energy	eV (*Nota bene!*)
$\delta(\beta\gamma)$	density effect correction to ionization energy loss	
$\hbar\omega_p$	plasma energy $\sqrt{4\pi N_e r_e^3}\; m_e c^2/\alpha$	$\sqrt{\rho\,\langle Z/A\rangle} \times 28.816$ eV $\hookrightarrow\ \rho$ in g cm^{-3}
N_e	electron density	(units of r_e)$^{-3}$
w_j	weight fraction of the jth element in a compound or mixture	
n_j	$\propto$ number of jth kind of atoms in a compound or mixture	
X_0	radiation length	g cm^{-2}
E_c	critical energy for electrons	MeV
$E_{\mu c}$	critical energy for muons	GeV
E_s	scale energy $\sqrt{4\pi/\alpha}\; m_e c^2$	21.2052 MeV
R_M	Molière radius	g cm^{-2}

33.2. Electronic energy loss by heavy particles [1–33]

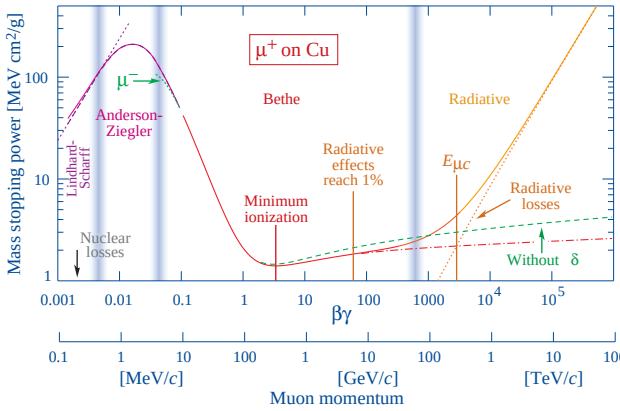

Figure 33.1: Mass stopping power ($= \langle -dE/dx \rangle$) for positive muons in copper as a function of $\beta\gamma = p/Mc$ over nine orders of magnitude in momentum (12 orders of magnitude in kinetic energy). Vertical bands indicate boundaries between different approximations discussed in the text.

33.2.2. *Maximum energy transfer in a single collision* :

For a particle with mass M,

$$W_{\rm max} = \frac{2m_e c^2\,\beta^2\gamma^2}{1 + 2\gamma m_e/M + (m_e/M)^2}\ . \tag{33.4}$$

33.2.3. *Stopping power at intermediate energies* :

The mean rate of energy loss by moderately relativistic charged heavy particles is well-described by the "Bethe equation,"

$$\left\langle -\frac{dE}{dx} \right\rangle = Kz^2 \frac{Z}{A}\frac{1}{\beta^2}\left[\frac{1}{2}\ln\frac{2m_e c^2\beta^2\gamma^2 W_{\rm max}}{I^2} - \beta^2 - \frac{\delta(\beta\gamma)}{2}\right]\ . \tag{33.5}$$

This is the *mass stopping power*; with the symbol definitions and values given in Table 33.1, the units are MeV $\rm g^{-1}cm^2$. $\langle -dE/dx \rangle$ defined in this way is about the same for most materials, decreasing slowly with Z. The *linear stopping power*, in MeV/cm, is $\langle -dE/dx \rangle\,\rho$, where ρ is the density in $\rm g/cm^3$.

As the particle energy increases, its electric field flattens and extends, so that the distant-collision contribution to Eq. (33.5) increases as $\ln\beta\gamma$. However, real media become polarized, limiting the field extension and effectively truncating this part of the logarithmic rise. Parameterization of the density effect term $\delta(\beta\gamma)$ in Eq. (33.5) is discussed in the full *Review* .

Few concepts in high-energy physics are as misused as $\langle dE/dx \rangle$. The mean is weighted by very rare events with large single-collision energy deposits. Even with samples of hundreds of events a dependable value for the mean energy loss cannot be obtained. Far better and more easily measured is the most probable energy loss, discussed below.

Although it must be used with cautions and caveats, $\langle dE/dx \rangle$ as described in Eq. (33.5) still forms the basis of much of our understanding

of energy loss by charged particles. Extensive tables are available [pdg.lbl.gov/AtomicNuclearProperties/].

Eq. (33.5) may be integrated to find the total (or partial) "continuous slowing-down approximation" (CSDA) range R. Since dE/dx depends (nearly) only on β, R/M is a function of E/M or pc/M.

33.2.9. ***Fluctuations in energy loss*** :

For detectors of moderate thickness x (*e.g.* scintillators or LAr cells), the energy loss probability distribution $f(\Delta; \beta\gamma, x)$ is adequately described by the highly-skewed Landau (or Landau-Vavilov) distribution [24,25]. The most probable energy loss

$$\Delta_p = \xi \left[\ln \frac{2mc^2\beta^2\gamma^2}{I} + \ln \frac{\xi}{I} + j - \beta^2 - \delta(\beta\gamma) \right] , \tag{33.11}$$

where $\xi = (K/2) \langle Z/A \rangle z^2 (x/\beta^2)$ MeV for a detector with a thickness x in g cm^{-2}, and $j = 0.200$ [26]. While dE/dx is independent of thickness, Δ_p/x scales as $a \ln x + b$. This most probable energy loss reaches a (Fermi) plateau rather than continuing $\langle dE/dx \rangle$'s lograthmic rise with increasing energy.

33.4. Photon and electron interactions in matter

At low energies electrons and positrons primarily lose energy by ionization, although other processes (Møller scattering, Bhabha scattering, e^+ annihilation) contribute. While ionization loss rates rise logarithmically with energy, bremsstrahlung losses rise nearly linearly (fractional loss is nearly independent of energy), and dominates above the critical energy (Sec. 33.4.4 below), a few tens of MeV in most materials

33.4.1. ***Collision energy losses by $e^{\pm}$*** :

Stopping power differs somewhat for electrons and positrons, and both differ from stopping power for heavy particles because of the kinematics, spin, charge, and the identity of the incident electron with the electrons that it ionizes. Complete discussions and tables can be found in Refs. 10, 11, and 29 in the full *Review*.

33.4.2. ***Radiation length*** :

High-energy electrons predominantly lose energy in matter by bremsstrahlung, and high-energy photons by e^+e^- pair production. The characteristic amount of matter traversed for these related interactions is called the radiation length X_0, usually measured in g cm^{-2}. X_0 has been calculated and tabulated by Y.S. Tsai [42]:

$$\frac{1}{X_0} = 4\alpha r_e^2 \frac{N_A}{A} \Big\{ Z^2 \big[L_{\rm rad} - f(Z) \big] + Z\, L'_{\rm rad} \Big\} . \tag{33.26}$$

For $A = 1$ g mol^{-1}, $4\alpha r_e^2 N_A/A = (716.408 \text{ g cm}^{-2})^{-1}$. $L_{\rm rad}$ and $L'_{\rm rad}$ are tabulated in the full *Review*, where a 4-place approximation for $f(z)$ is also given.

33.4.3. ***Bremsstrahlung energy loss by $e^{\pm}$*** :

At very high energies and except at the high-energy tip of the bremsstrahlung spectrum, the cross section can be approximated in the "complete screening case" as [42]

$$\begin{aligned} d\sigma/dk = (1/k) 4\alpha r_e^2 \big\{ &(\tfrac{4}{3} - \tfrac{4}{3}y + y^2) [Z^2 (L_{\rm rad} - f(Z)) + Z\, L'_{\rm rad}] \\ &+ \tfrac{1}{9}(1-y)(Z^2+Z) \big\} , \end{aligned} \tag{33.29}$$

where $y = k/E$ is the fraction of the electron's energy transferred to the radiated photon. At small y (the "infrared limit") the term on the second

line ranges from 1.7% (low Z) to 2.5% (high Z) of the total. If it is ignored and the first line simplified with the definition of X_0 given in Eq. (33.26), we have

$$\frac{d\sigma}{dk} = \frac{A}{X_0 N_A k}\left(\tfrac{4}{3} - \tfrac{4}{3}y + y^2\right) \ . \tag{33.30}$$

33.4.4. *Critical energy* :

An electron loses energy by bremsstrahlung at a rate nearly proportional to its energy, while the ionization loss rate varies only logarithmically with the electron energy. The *critical energy* E_c is sometimes defined as the energy at which the two loss rates are equal [49]. Among alternate definitions is that of Rossi [2], who defines the critical energy as the energy at which the ionization loss per radiation length is equal to the electron energy. Equivalently, it is the same as the first definition with the approximation $|dE/dx|_{\rm brems} \approx E/X_0$. This form has been found to describe transverse electromagnetic shower development more accurately.

Values of E_c for electrons can be reasonaby well described by (610 MeV)/$(Z + 1.24)$ for solids and (710 MeV)/$(Z + 0.92)$ for gases. E_c for both electrons and positrons in more than 350 materials can be found at `pdg.lbl.gov/AtomicNuclearProperties`.

33.4.5. *Energy loss by photons* :

At low energies the photoelectric effect dominates, although Compton scattering, Rayleigh scattering, and photonuclear absorption also contribute. The photoelectric cross section is characterized by discontinuities (absorption edges) as thresholds for photoionization of various atomic levels are reached. Pair production dominates at high energies, but is supressed at ultrahigh energies because of quantum mechanical interference between amplitudes from different scattering centers (LPM effect).

At still higher photon and electron energies, where the bremsstrahlung and pair production cross-sections are heavily suppressed by the LPM effect, photonuclear and electronuclear interactions predominate over electromagnetic interactions. At photon energies above about 10^{20} eV, for example, photons usually interact hadronically.

33.5. Electromagnetic cascades

When a high-energy electron or photon is incident on a thick absorber, it initiates an electromagnetic cascade as pair production and bremsstrahlung generate more electrons and photons with lower energies.

The longitudinal development is governed by the high-energy part of the cascade, and therefore scales as the radiation length in the material. Electron energies eventually fall below the critical energy, and then dissipate their energy by ionization and excitation rather than by the generation of more shower particles. In describing shower behavior, it is convenient to introduce the scale variables

$$t = x/X_0 \ , \qquad\qquad y = E/E_c \ , \tag{33.35}$$

so that distance is measured in units of radiation length and energy in units of critical energy.

The mean longitudinal profile of the energy deposition in an electromagnetic cascade is reasonably well described by a gamma distribution [59],

$$\frac{dE}{dt} = E_0\, b\, \frac{(bt)^{a-1}e^{-bt}}{\Gamma(a)} \ , \tag{33.36}$$

at energies from 1 GeV to 100 GeV.

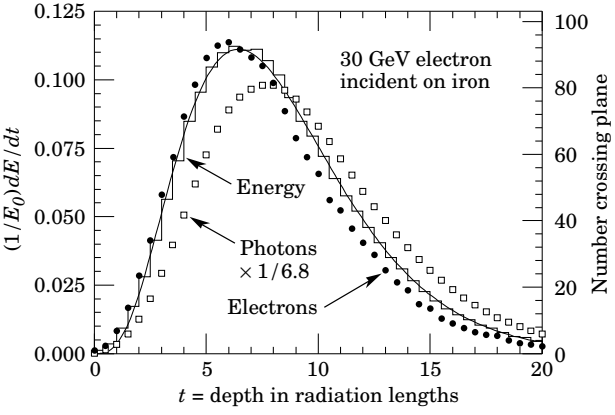

Figure 33.20: An EGS4 simulation of a 30 GeV electron-induced cascade in iron. The histogram shows fractional energy deposition per radiation length, and the curve is a gamma-function fit to the distribution.

33.6. Muon energy loss at high energy

At sufficiently high energies, radiative processes become more important than ionization for all charged particles. These contributions increase almost linearily with energy. It is convenient to write the average rate of muon energy loss as [72]

$$-dE/dx = a(E) + b(E)\,E\ . \tag{33.41}$$

Here $a(E)$ is the ionization energy loss given by Eq. (33.5), and $b(E)\,E$ is the sum of e^+e^- pair production, bremsstrahlung, and photonuclear contributions. These are subject large fluctuations, particularly at higher energies.

To the approximation that the slowly-varying functions $a(E)$ and $b(E)$ are constant, the mean range x_0 of a muon with initial energy E_0 is given by

$$x_0 \approx (1/b)\ln(1 + E_0/E_{\mu c})\ , \tag{33.42}$$

where $E_{\mu c} = a/b$.

The "muon critical energy" $E_{\mu c}$ can be defined as the energy at which radiative and ionization losses are equal, and can be found by solving $E_{\mu c} = a(E_{\mu c})/b(E_{\mu c})$. This definition is different from the Rossi definition we used for electrons. It decreases with Z, and is several hundred GeV for iron. It is given for the elements and many other materials in `pdg.lbl.gov/AtomicNuclearProperties`.

33.7. Cherenkov and transition radiation

A charged particle radiates if its velocity is greater than the local phase velocity of light (Cherenkov radiation) or if it crosses suddenly from one medium to another with different optical properties (transition radiation). Neither process is important for energy loss, but both are used in high-energy and cosmic-ray physics detectors.

33.7.1. ***Optical Cherenkov radiation*** :

The angle θ_c of Cherenkov radiation, relative to the particle's direction, for a particle with velocity βc in a medium with index of refraction n is

$$\begin{aligned} \cos\theta_c &= (1/n\beta) \\ \text{or} \quad \tan\theta_c &= \sqrt{\beta^2 n^2 - 1} \\ &\approx \sqrt{2(1-1/n\beta)} \quad \text{for small } \theta_c, \textit{e.g.} \text{ in gases.} \end{aligned} \tag{33.43}$$

The threshold velocity β_t is $1/n$. Values of $n-1$ for various commonly used gases are given as a function of pressure and wavelength in Ref. 78. Data for other commonly used materials are given in Ref. 79.

The number of photons produced per unit path length of a particle with charge ze and per unit energy interval of the photons is

$$\begin{aligned} \frac{d^2N}{dEdx} &= \frac{\alpha z^2}{\hbar c}\sin^2\theta_c = \frac{\alpha^2 z^2}{r_e\, m_e c^2}\left(1 - \frac{1}{\beta^2 n^2(E)}\right) \\ &\approx 370\, \sin^2\theta_c(E)\ \text{eV}^{-1}\text{cm}^{-1} \qquad (z=1)\ , \end{aligned} \tag{33.45}$$

or, equivalently,

$$\frac{d^2N}{dxd\lambda} = \frac{2\pi\alpha z^2}{\lambda^2}\ \left(1 - \frac{1}{\beta^2 n^2(\lambda)}\right)\ . \tag{33.46}$$

33.7.2. ***Coherent radio Cherenkov radiation*** :

Coherent Cherenkov radiation is produced by many charged particles with a non-zero net charge moving through matter on an approximately common "wavefront"—for example, the electrons and positrons in a high-energy electromagnetic cascade. Near the end of a shower, when typical particle energies are below E_c (but still relativistic), a charge imbalance develops. Photons can Compton-scatter atomic electrons, and positrons can annihilate with atomic electrons to contribute even more photons which can in turn Compton scatter. These processes result in a roughly 20% excess of electrons over positrons in a shower. The net negative charge leads to coherent radio Cherenkov emission. The phenomenon is called the Askaryan effect [84]. The signals can be visible above backgrounds for shower energies as low as 10^{17} eV; see Sec. 35.3.3 for more details.

33.7.3. ***Transition radiation*** :

The energy radiated when a particle with charge ze crosses the boundary between vacuum and a medium with plasma frequency ω_p is

$$I = \alpha z^2 \gamma \hbar\omega_p/3\ . \tag{33.47}$$

The plasma energy $\hbar\omega_p$ is defined in Table 33.1.

For styrene and similar materials, $\hbar\omega_p \approx 20$ eV; for air it is 0.7 eV. The number spectrum $dN_\gamma/d(\hbar\omega$ diverges logarithmically at low energies and decreases rapidly for $\hbar\omega/\gamma\hbar\omega_p > 1$. Inevitable absorption in a practical detector removes the divergence. About half the energy is emitted in the range $0.1 \le \hbar\omega/\gamma\hbar\omega_p \le 1$. The γ dependence of the emitted energy thus comes from the hardening of the spectrum rather than from an increased quantum yield. For a particle with $\gamma = 10^3$, the radiated photons are in the soft x-ray range 2 to 40 keV.

The number of photons with energy $\hbar\omega > \hbar\omega_0$ is given by the answer to problem 13.15 in Ref. 33,

$$N_\gamma(\hbar\omega > \hbar\omega_0) = \frac{\alpha z^2}{\pi}\left[\left(\ln\frac{\gamma\hbar\omega_p}{\hbar\omega_0} - 1\right)^2 + \frac{\pi^2}{12}\right]\ , \tag{33.49}$$

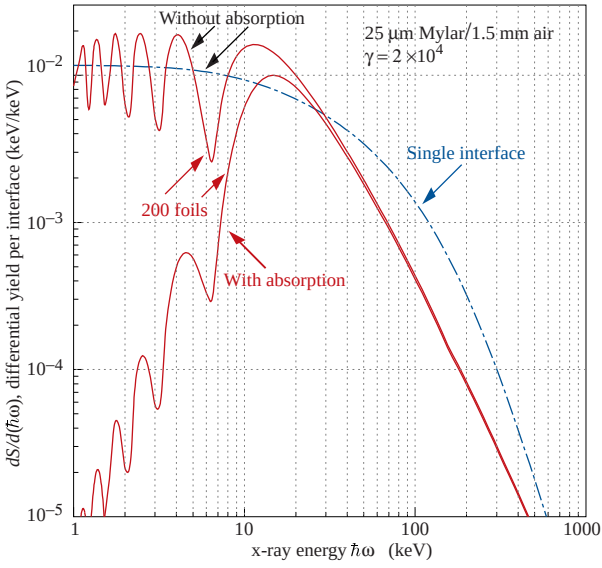

Figure 33.27: X-ray photon energy spectra for a radiator consisting of 200 25 μm thick foils of Mylar with 1.5 mm spacing in air (solid lines) and for a single surface (dashed line).

within corrections of order $(\hbar\omega_0/\gamma\hbar\omega_p)^2$. The number of photons above a fixed energy $\hbar\omega_0 \ll \gamma\hbar\omega_p$ thus grows as $(\ln\gamma)^2$, but the number above a fixed fraction of $\gamma\hbar\omega_p$ (as in the example above) is constant. For example, for $\hbar\omega > \gamma\hbar\omega_p/10$, $N_\gamma = 2.519\,\alpha z^2/\pi = 0.0059 \times z^2$.

The particle stays "in phase" with the x ray over a distance called the formation length, $d(\omega) = (2c/\omega)(1/\gamma^2 + \theta^2 + \omega_p^2/\omega^2)^{-1}$. Most of the radiation is produced in this distance. Here θ is the x-ray emission angle, characteristically $1/\gamma$. For $\theta = 1/\gamma$ the formation length has a maximum at $d(\gamma\omega_p/\sqrt{2}) = \gamma c/\sqrt{2}\,\omega_p$. In practical situations it is tens of μm.

Since the useful x-ray yield from a single interface is low, in practical detectors it is enhanced by using a stack of N foil radiators—foils L thick, where L is typically several formation lengths—separated by gas-filled gaps. The amplitudes at successive interfaces interfere to cause oscillations about the single-interface spectrum. At increasing frequencies above the position of the last interference maximum ($L/d(w) = \pi/2$), the formation zones, which have opposite phase, overlap more and more and the spectrum saturates, $dI/d\omega$ approaching zero as $L/d(\omega) \to 0$. This is illustrated in Fig. 33.27 for a realistic detector configuration.

Although one might expect the intensity of coherent radiation from the stack of foils to be proportional to N^2, the angular dependence of the formation length conspires to make the intensity $\propto N$.

34. Particle Detectors at Accelerators

34.1. Introduction

This review summarizes the detector technologies employed at accelerator particle physics experiments. Several of these detectors are also used in a non-accelerator context and examples of such applications will be provided. The detector techniques which are specific to non-accelerator particle physics experiments are the subject of Chap. 35. More detailed discussions of detectors and their underlying physics can be found in books by Ferbel [1], Kleinknecht [2], Knoll [3], Green [4], Leroy & Rancoita [5], and Grupen [6].

In Table 34.1 are given typical resolutions and deadtimes of common charged particle detectors. The quoted numbers are usually based on typical devices, and should be regarded only as rough approximations for new designs. The spatial resolution refers to the intrinsic detector resolution, i.e. without multiple scattering. We note that analog detector readout can provide better spatial resolution than digital readout by measuring the deposited charge in neighboring channels. Quoted ranges attempt to be representative of both possibilities. The time resolution is defined by how accurately the time at which a particle crossed the detector can be determined. The deadtime is the minimum separation in time between two resolved hits on the same channel. Typical performance of calorimetry and particle identification are provided in the relevant sections below.

Table 34.1: Typical resolutions and deadtimes of common charged particle detectors. Revised November 2011.

Detector Type	Intrinsinc Spatial Resolution (rms)	Time Resolution	Dead Time
Resistive plate chamber	$\lesssim$10 mm	1 ns (50 ps[a])	—
Streamer chamber	300 μm[b]	2 μs	100 ms
Liquid argon drift [7]	$\sim$175–450 μm	$\sim$ 200 ns	$\sim$ 2 μs
Scintillation tracker	$\sim$100 μm	100 ps/n[c]	10 ns
Bubble chamber	10–150 μm	1 ms	50 ms[d]
Proportional chamber	50–100 μm[e]	2 ns	20-200 ns
Drift chamber	50–100 μm	2 ns[f]	20-100 ns
Micro-pattern gas detectors	30–40 μm	$<$ 10 ns	10-100 ns
Silicon strip	pitch/(3 to 7)[g]	few ns[h]	$\lesssim$50 ns[h]
Silicon pixel	$\lesssim$10 μm	few ns[h]	$\lesssim$50 ns[h]
Emulsion	1 μm	—	—

[a] For multiple-gap RPCs.
[b] 300 μm is for 1 mm pitch (wirespacing/$\sqrt{12}$).
[c] n = index of refraction.
[d] Multiple pulsing time.
[e] Delay line cathode readout can give $\pm$150 μm parallel to anode wire.
[f] For two chambers.
[g] The highest resolution ("7") is obtained for small-pitch detectors ($\lesssim$25 μm) with pulse-height-weighted center finding.
[h] Limited by the readout electronics [8].

Further discussion and all references may be found in the full *Review*.